# Influence of the Junction Capacitance of the Secondary Rectifier Diodes on Output Characteristics in Multi-Resonant Converters

Stefan Ditze, Thomas Heckel, Martin März
Fraunhofer Institute for Integrated Systems and Device Technology IISB
Schottkystrasse 10, 91058 Erlangen, Germany
stefan.ditze@iisb.fraunhofer.de

***Abstract*— Multi-resonant converters like the CLLLC topology are known for their outstanding efficiency and high power density. Little information has however been published about the influences of secondary side diode junction capacitances on the output characteristics of the resonant converter. This paper presents a detailed analysis of these influences in the inductive working range and reviews practical design considerations of the converter. Therefore, experimental results of an inductive power transfer system, using a CLLLC resonant topology, are compared to theoretical time domain solution, showing significant effects of different semiconductor materials and devices on output power. These effects will be discussed and explained in detail by using measured key waveforms.**

***Keywords—Parasitic components; output rectifier; transistor output capacitance; diode junction capacitance; CLLLC resonant converter; time domain solution***

## I. INTRODUCTION

Besides the well-established group of galvanically isolated power converters, e.g. forward or push-pull converters, the group of resonant converters are gaining more and more interest in the last years [1]-[3]. The main advantage of the resonant converter is reduced switching losses, due to the soft switching capability of the primary inverter switches. This enables operation at high switching frequencies $f_{sw}$, resulting in smaller inductive component sizes and hence in low overall converter size and high power density [4], [5]. However, the development of resonant converters is challenging for most designers, due to the resonant operating principle. Especially, the multi resonant behavior of the CLLLC resonant converter (Fig. 1) and also the LLC resonant converter (not shown) presents a considerable obstacle during the design process. Resonant converters can be implemented by employing either unidirectional (Fig. 1(a)) or bidirectional (Fig. 1(b)) switches on the secondary side. Thereby, the unidirectional configuration is often used for applications in galvanically isolated switch-mode power supplies [6], [7]. For systems in which a bidirectional energy transfer is required, e.g. between two DC grids, connection of a HV battery storage to a DC bus, or battery chargers, the bidirectional configuration is applied [8]-[10]. Depending on the present application, both configurations are used in inductive power transfer (IPT) systems [11]-[14].

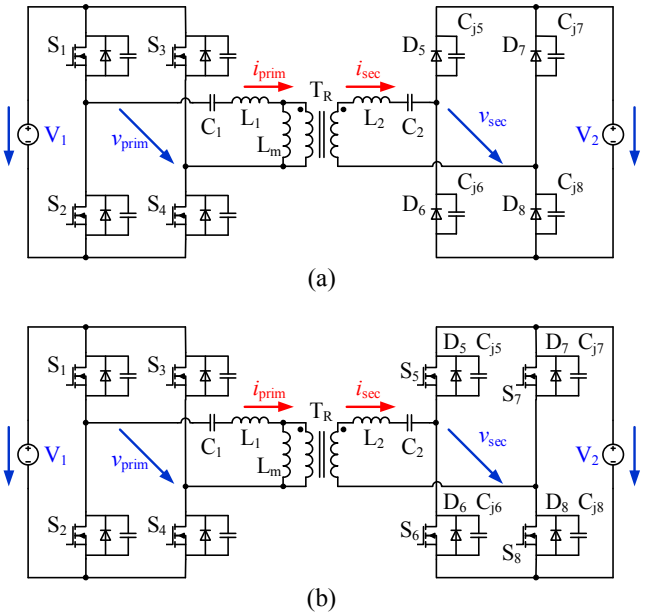


Fig. 1. Topology of the CLLLC resonant converter with (a) unidirectional switches and (b) bidirectional switches on the secondary side.

Precise knowledge of the characteristics and performance of the resonant converter is therefore necessary in order to achieve the optimum performance of the converter for a given application. As rather straightforward approach resonant converters can be analyzed theoretically by the first harmonic approximation (FHA) method, assuming that only sinusoidal current waveforms are applied on the resonant tank and only ideal components are utilized [15]. A more detailed and advanced analysis is the calculation of the time domain solution (TDS) for steady-state [16], [17]. But it has been shown that there is still a deviation between measurement and TDS calculation [17], which is merely not explainable with resistive losses and/or dead time of the primary inverter. Both methods, FHA and TDS, have the disadvantage that they do not account for the secondary side rectifier diodes junction capacitances and their significant influences on converter output characteristic, which represents the most important point for design considerations. In literature the influence of the

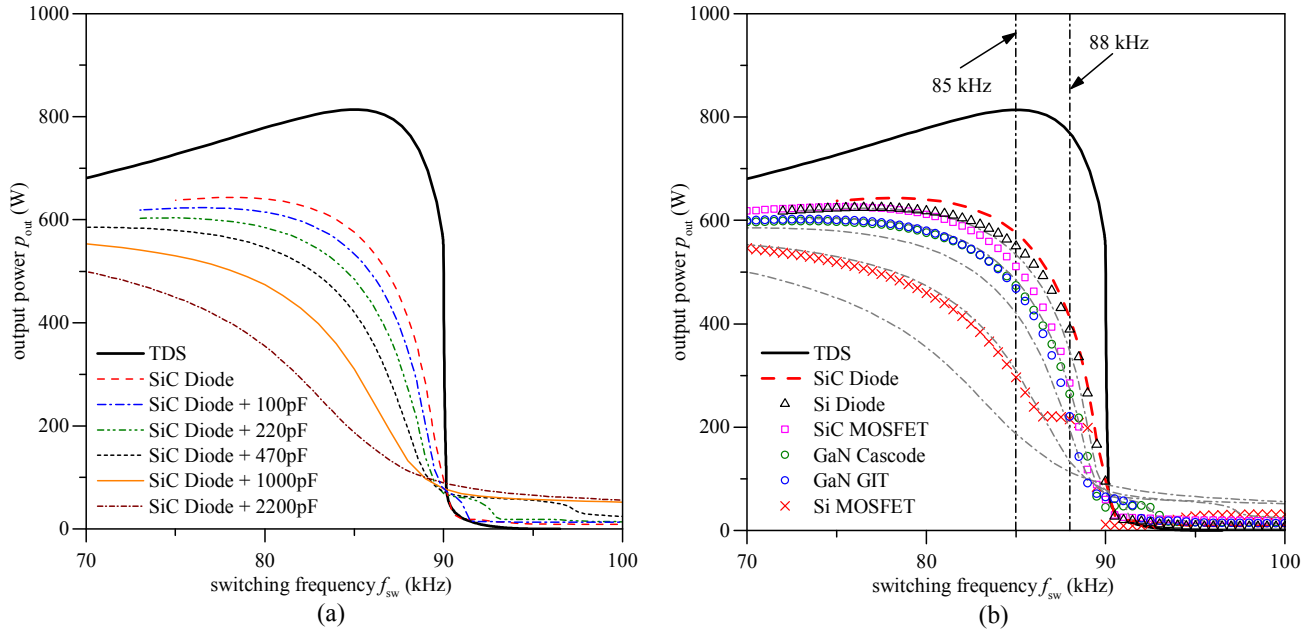


Fig. 2. Measured output power characteristics $p_{out}$ plotted against switching frequency $f_{sw}$ of an IPT system in step-up operation mode with $V_{in} = 200$ V and $V_{out} = 220$ V. Reference measurements using SiC Schottky barrier diode (SiC SBD) as bridge rectifier with additional capacitances parallel to each diode are depicted in (a). Measurements with SiC diode, SiC MOSFET, GaN transistors, Si diode, and Si MOSFET used as secondary side bridge rectifier are shown in (b).

junction capacitance on output power is only rarely discussed. Chen et al. analyze the influence of the secondary side junction capacitances only on zero-voltage switching (ZVS) of the primary inverter switches [18], whereas Kim et al. analyze the influence of secondary side junction capacitance on output voltage, but only at very light load and without differentiation between step-down and step-up operation mode [19]. Other authors discuss the influence of the junction capacitances only rudimentary within the scope of loss analysis in resonant converters [20]-[22].

In this paper the influence of the secondary side rectifier diodes junction capacitance on converter output power is analyzed, by comparing experimental results of an exemplary IPT system, using a CLLLC topology, with TDS calculations. Different devices for unidirectional and bidirectional operating mode and different materials, e.g. SiC, GaN, or Si, are investigated in detail, showing significant effects on converter output power. Based on this knowledge practical design considerations for a series resonant converter are provided for both unidirectional and bidirectional CLLLC topology.

## II. Measurements of the Influence of the Rectifier Diodes Junction Capacitance on $P_{OUT}$

In this section the output power characteristics in step-up (Fig. 2) and step-down (Fig. 3) operation mode for different Si and wide-bandgap semiconductor devices for an exemplary IPT system are presented and compared to TDS calculations. Depending on the semiconductor device and material the value of the diode junction capacitance $C_j$ and the transistor output capacitance $C_{oss}$ range between several picofarad to a few nanofarad [23]. Furthermore, the capacitance values vary with the applied diode voltage and drain source voltage, respectively. Due to bipolar device effects in Si devices, the comparison with equivalent capacitance values is just valid for the given operating point as temperature, switching current, and current slope alter the effective capacitance value [24]. Measurements with a SiC Schottky barrier diode (SiC SBD) are carried out as a reference (Fig. 2(a) and Fig. 3(a)). The used SiC SBD performs almost like an ideal diode, because of the low junction capacitance and its unipolar behavior [25], [26]. Adding additional discrete capacitances $C_{add}$ in parallel to each SiC SBD on the secondary side allows estimating the equivalent capacitance value for the different used Si and wide-bandgap semiconductors.

### *A. Step-up operation mode*

First, the output power characteristics in step-up operation mode for a SiC SBD and SiC SBD with additional discrete capacitances (Fig. 2(a)) and different Si and wide-bandgap semiconductor devices (Fig. 2(b)) as secondary side rectifier for an exemplary IPT system with $V_{in} = 200$ V, $V_{out} = 220$ V, and an inductive coupling factor $k = 0.7$ are shown. For comparison, TDS calculations for the exemplary chosen operating point with ideal components are plotted. To begin with, the reference measurements in Fig. 2(a) are described. With increasing values of the additional discrete capacitance, a more substantial deviation from TDS calculation is observed. The measured output power gets significantly lower, which consequently results in a decreased output power capability in step-up mode. Moreover, the switching frequency at which the resonant converter can be regulated down to zero output power shifts towards higher frequencies. Furthermore, for values $C_{add}$ greater than 1000 pF it is not possible to achieve zero output power by increasing the switching frequency $f_{sw}$ for the exemplary IPT system. Because under very light load conditions the stray inductance $L_1$ (respectively $L_2$) and the rectifier diodes capacitances form a series resonant LC circuit

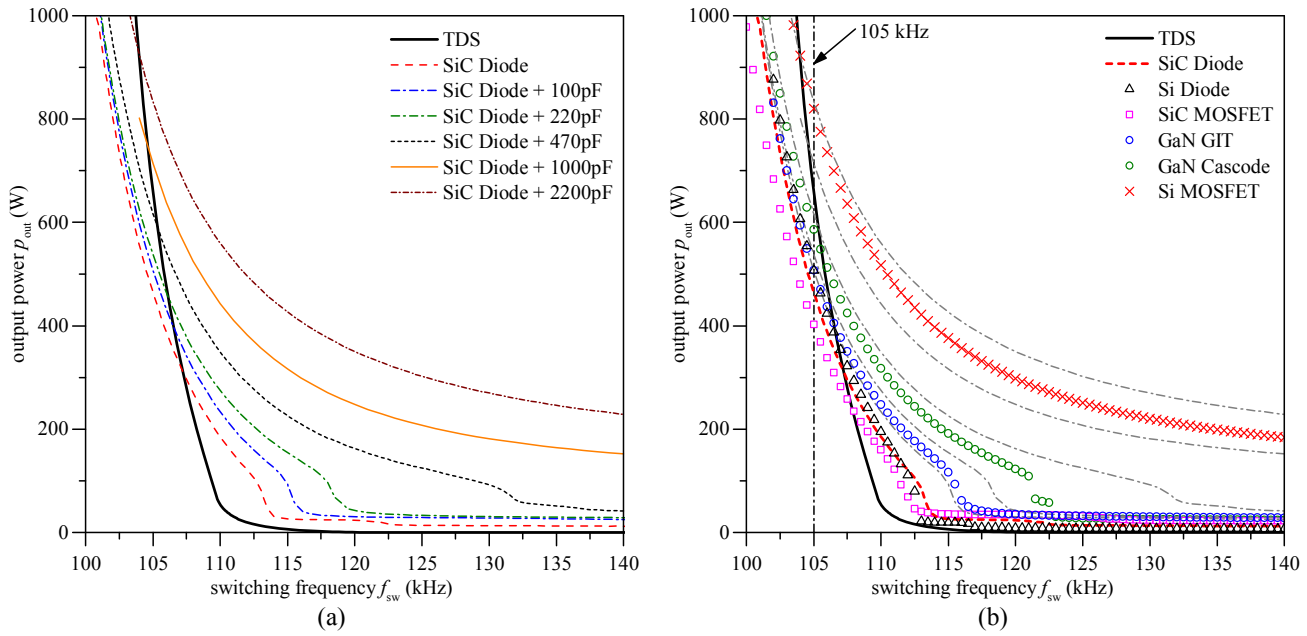


Fig. 3. Measured output power characteristics $p_{out}$ plotted against switching frequency $f_{sw}$ of an IPT system in step-down operating mode with $V_{in}$ = 200 V and $V_{out}$ = 180 V. Reference measurements using SiC SBD bridge rectifier with additional capacitances parallel to each diode are depicted in (a). Measurements with SiC SBD, SiC MOSFET, GaN transistors, Si diode, and Si MOSFET used as secondary side bridge rectifier are shown in (b).

which transfers energy to the secondary side driven by the voltage transition of the primary inverter and prevents to achieve zero output power [19]. In addition, the minimum frequency, where ZVS for the primary inverter is still achievable, decreases also with increasing capacitance values ($C_j + C_{add}$) of the output rectifier diodes. Further, for some reference measurements a bend in the measured curves is observed at switching frequencies greater than 90 kHz, which is explained by a change of the operating mode.

Next, the output power characteristics in step-up operation mode of the different semiconductor devices and materials are described in Fig. 2(b). Here, measurements for a SiC MOSFET (pink squares), GaN transistors (blue and green circles), Si diode (black triangles) and Si super-junction MOSFET (red crosses) as secondary side rectifier are depicted, which represent the state of the art power semiconductors. The investigated semiconductors and their calculated time-related equivalent capacitances $C_{eq,tr}$ using the $C_j(V_R)$, respectively $C_{oss}(V_{ds})$, measurements in the corresponding datasheet are listed in Table I [4]. For comparison the reference measurements with the SiC SBD (red dashes) and SiC SBD with additional discrete capacitances (grey dashed lines) are included. This allows estimating the capacitance values of the different semiconductor devices in the framework of the experimental set-up in step-up operation mode. Further, the comparison to datasheet values is also possible (see Table I).

As expected, the output power characteristics in step-up operation mode deviate substantially for all applied secondary side rectifier semiconductors from TDS calculation (Fig. 2(b)). Obviously, the measured output power gets significantly lower, with increasing values of the capacitance. This indicates that the influence of the secondary side rectifier diodes junction capacitance on converter output power should not be neglected for the design of a resonant converter. The greatest deviation from TDS calculation is observed for the Si MOSFET (red crosses), due to its large output capacitance (about 1 nF, see Table I), its bipolar body diode and the reverse recovery characteristic of the device. Further, a discontinuity is observed at part load between 86 kHz and 90 kHz, which is not just a change of the operating mode as mentioned before. This special effect of the Si MOSFET device will be explained later

TABLE I. EXTRACTED DATASHEET VALUES FOR STEP-UP AND STEP-DOWN OPERATION MODE OF VARIOUS DEVICES

| **Device** | | **$C_{eq,tr}$ (pF)** | |
|---|---|---|---|
| | | **Step-Up Mode** | **Step-Down Mode** |
| C3D20060D[a] | SiC diode, 600V | 81 | 89 |
| VS-APU3006-F3[b] | Si diode, ultrafast, 600V | 45 | 49 |
| C2M0160120D[c] | SiC MOSFET, 1200V, 160mΩ | 124 | 135 |
| - | Normally-off GaN HEMT, 600V, 40mΩ | 333 | 354 |
| TPH3205WS[d] | Cascode GaN HEMT, 600V, 52mΩ | 428 | 485 |
| IPW65R110CFD[e] | MOSFET, 650V, 110mΩ | 1040 | 1239 |

a. Cree, Silicon Carbide Schottky Diode Z-Rec™ Rectifier C3D20060D, Datasheet, Rev. C, 2012. *(Derived from $C_j$, refers to 220V, respectively 180V)*

b. Vishay Semiconductors, Ultrafast Rectifier, 30A FRED Pt® VS-APU3006-F3, Datasheet, Rev. 17-Jul-13. *(Derived from $C_j$, refers to 220V, respectively 180V)*

c. Cree, Silicon Carbide Power MOSFET C2M™ MOSFET Technology C2M0160120D, Datasheet, Rev. June 16, 2015 JH. *(Derived from $C_{oss}$, refers to 220V, respectively 180V)*

d. Transphorm, GaN Power Low-loss Switch TPH3205WS, Datasheet, Rev. C, 2012. *(Derived from $C_{oss}$, refers to 220V, respectively 180V)*

e. Infineon Technologies AG, 650V CoolMOS™ CFD2 Power Transistor IPW65R110CFD, Datasheet, Rev. 2.6, 2011-09-26. *(Derived from $C_{oss}$, refers to 220V, respectively 180V)*

on the basis of measured current and voltage waveforms of the resonant tank. For the other power semiconductors the deviation from TDS calculation is equally large. As expected from the comparable values of equivalent capacitance $C_{eq,tr}$ from Table I, the measured characteristic of the SiC MOSFET (pink squares) is very similar to the measured reference SiC SBD curve. In contrast to Si counterparts, measurements of the turn-off behavior of the SiC MOSFET body diode have shown a nearly capacitive and unipolar characteristic [27]. Hence, the output power curve of the SiC MOSFET fits well to the reference measurement with an additional capacitance of $C_{add} = 100$ pF. The Si diode is a performance optimized ultrafast diode and shows a great performance with a small junction capacitance (black tringles), similar to the reference SiC SBD. However, at low switching frequencies the reverse recovery effect of the Si diode commences which results in a virtual increase of the diode junction capacitance and the measured curve falls below the reference SiC SBD curve. In contrast to Si semiconductors, GaN high electron mobility transistors (HEMT) offer a much lower gate charge and a smaller junction capacitance due to their lateral structure [28], [29]. Two kinds of GaN HEMT are available which are suitable for power electronic applications: the normally-off (enhancement) GaN HEMT and the cascode GaN HEMT, which utilizes a low voltage Si MOSFET in series with a normally-on (depletion) GaN HEMT. The cascode structure has the advantage of simplified gate driving compared to the single GaN based normally-off device because of the higher driving safety margin (cascode: $v_{GSS} = \pm 18$ V, normally-off GaN HEMT: $v_{GSS} = -10$ V…+4 V). The GaN transistors have nearly identical output power curves, only at switching frequencies higher than 90 kHz a discontinuity for the cascode GaN HEMT is observed, similar to the Si MOSFET. This may result from the fact that the body diode of the Si MOSFET conducts if the cascode GaN HEMT is operated in reverse mode. Compared to the datasheet value in Table I the estimated capacitance value from the experimental set-up of the cascode GaN HEMT is lower. Further research has to be conducted to evaluate if this results from e.g. cascode related effects or deviations from the device and the datasheet characteristics.

### B. Step-down operation mode

The former described measurements are also performed for the step-down mode for the IPT system with $V_{in} = 200$ V and $V_{out} = 180$ V (Fig. 3). TDS calculations for the exemplary chosen operating point with ideal components are also plotted. In contrast to the step-up mode the measured output power is significantly higher at high switching frequencies and the curve progression of $p_{out}$ rises less steep with decreasing switching frequencies for the reference SiC SBD and the different semiconductors than TDS calculation predicts. Hence, also for step-down operation mode, it is important to consider the secondary side rectifier diodes junction capacitance for the design of a resonant converter. Besides these differences for the step-down mode nearly the same effects as for the step-up mode are observed. With increasing $C_{add}$ the deviation for the reference measurements from TDS gets larger, the output power rises significantly and thus zero output power cannot be achieved at high switching frequencies for values $C_{add}$ greater than 1000 pF (Fig.3 (a)). Further, the above described bends in $p_{out}$ progression are also observed at switching frequencies greater than 110 kHz and indicate operating mode changes (Fig.3 (a)). Again, for the Si MOSFET the biggest deviation from TDS is observed (Fig. 3(b)). However, at part load a discontinuity is not found for investigated switching frequencies up to 400 kHz. Further, the reverse recovery effect of the Si diode commences also at low switching frequencies, which results in a virtual increase of the diode junction capacitance and thus the measured $p_{out}$ curve rises above the reference SiC SBD curve. For the normally-off GaN transistor a difference in step-down mode is observed. The measurement shows, that the estimated capacitance value from the experimental set-up is much lower than the calculated datasheet value.

## III. Discussion and Results

In order to explain the observed output power characteristics, measured key waveforms of the resonant tank in step-up and step-down operation mode are analyzed.

### A. Subintervals and operating modes

In multi-resonant topologies more than one resonant frequency exists which leads to different resonant stages within one switching cycle. These resonant stages, in the following called subintervals, are characterized by the condition of the output rectifier. First, the individual subintervals are briefly discussed (Fig. 4) as this will be important for the following discussion. For a more detailed description please refer to [16] for the LLC and to [17] for the CLLLC topology. Within one

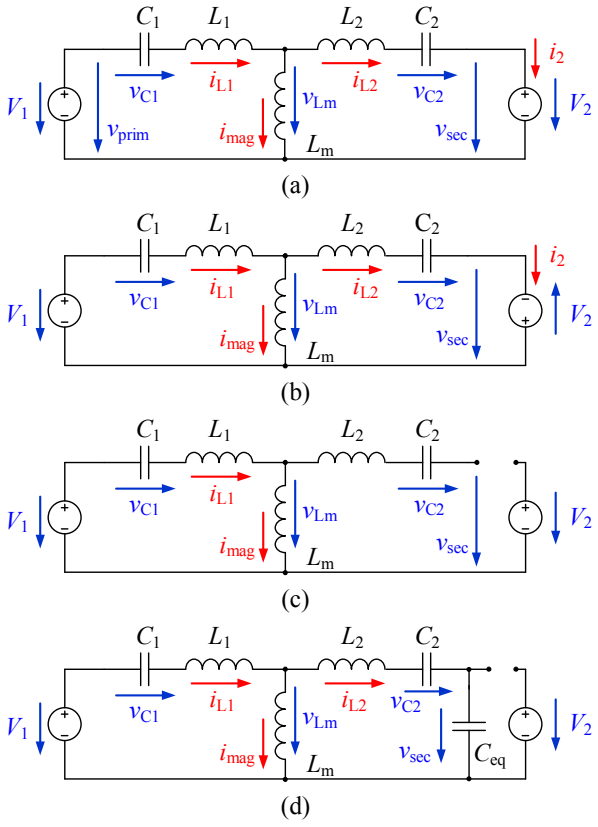


Fig. 4. CLLLC resonant tank equivalent circuits for the first half-cycle switching period. (a) Subinterval P. (b) Subinterval N. (c) Subinterval O. (d) Subinterval D.

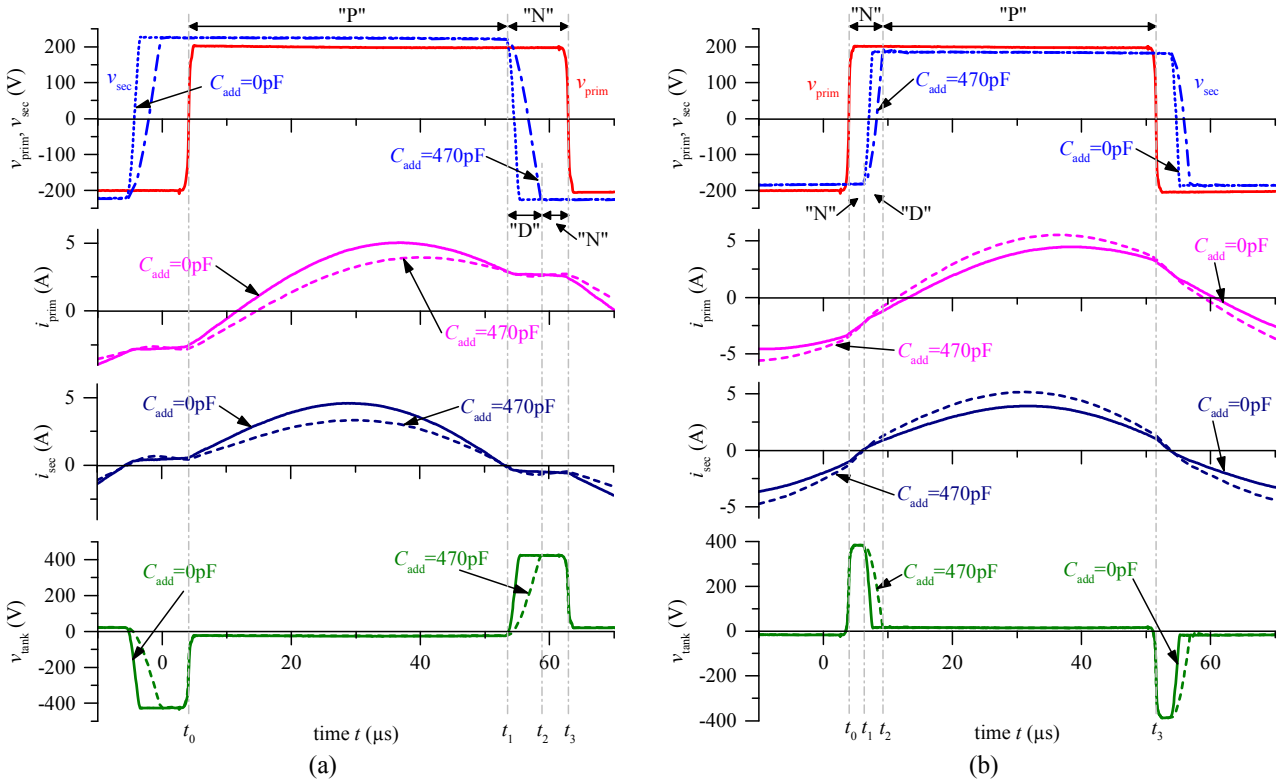


Fig. 5. Measured key waveforms for step-up operation mode with $V_{in}$ = 200 V and $V_{out}$ = 220 V at $f_{sw}$ = 85 kHz (a) and for step-down operation mode with $V_{in}$ = 200 V and $V_{out}$ = 180 V at $f_{sw}$ = 105 kHz (b). For the measurements the reference SiC SBD (solid lines) and the reference SiC SBD with additional capacitance Cadd = 470 pF parallel to each diode are used (dashed lines).

half-cycle of the switching period $T_S$ the polarity of the secondary resonant voltage $v_{sec}$ can be positive (subinterval P), negative (subinterval N), or undefined due to the blocking state of all rectifier diodes (subinterval O). Additional to these subintervals, a new subinterval D has to be introduced, considering the diode junction capacitances. In the subsequent second half-cycle these subintervals occur as well with inverse algebraic signs in resonant tank currents and voltages. In subinterval P, the output rectifier conducts and applies $+V_2$ to the secondary side resonant tank $L_m$-$L_2$-$C_2$ (Fig. 4(a)). The primary current $i_{prim}$ starts to rise in a sinusoidal shape and exceeds the magnetizing current $i_{mag}$. Therefore, power is delivered to the secondary side as the secondary resonant current $i_{sec} = i_{prim} - i_{mag}$ is positive. Similar to subinterval P, in subinterval N the conducting secondary side rectifier applies $-V_2$ to the secondary resonant tank $L_m$-$L_2$-$C_2$ which reduces $i_{prim}$ and thus $i_{sec}$ in a sinusoidal manner (Fig. 4(b)). Hence, the output power diminishes until $i_{sec}$ crosses zero and subinterval N ends. In contrast to the former discussed subintervals, in subinterval O all rectifier diodes on the secondary side are OFF and thus no current flow into the decoupled output voltage source is established (Fig. 4(c)). The new subinterval D bases on subinterval O, but considers the diode junction capacitance of the applied non-ideal unidirectional or bidirectional switch. In stage D, all rectifier diodes block and decouple $V_2$ from the resonant tank. However, the secondary resonant tank $L_m$-$L_2$-$C_2$ is connected to the parasitic diode junction capacitance which is charged to $v_{sec} = \pm V_2$ depending on the preceding subinterval. The diode junction capacitances are discharged (respectively charged) to the output voltage with inverse algebraic sign by the secondary current $i_{sec}$. Thus, also no output power is transferred to the load and stage D ends as soon as the discharge (respectively charge) process is finished (Fig. 4(d)). Different combinations of the previously discussed subintervals form several operating modes in which the CLLLC converter works in step-up and step-down operation mode. These operating modes are named after the involved subintervals, e.g. in operating mode NP, subinterval P follows after subinterval N. Under the assumption of ideal components and semiconductor devices the subintervals N, P, and O built seven operating modes, namely PN, PON, PO, OPO, and O in step-up operation mode and PN, NP, NOP, OPO, and O in step-down mode. If the subinterval D is also included even more operating modes are possible. The transitions between the different operating modes occur as a function of the switching frequency and load conditions. Hence, the operating mode transition can be observed as the measured or calculated output power $p_{out}$ characteristic alters its gradient.

### *B. New subinterval D in step-up operation mode*

In the following, the new subinterval D is discussed in detail. Figure 5 shows the measured primary $v_{prim}$ and secondary $v_{sec}$ voltage and also the primary $i_{prim}$ and secondary $i_{sec}$ current at the resonant tank for the reference SiC SBD (solid lines) and for the SiC SBD with additional capacitance $C_{add}$ (dashed lines). The step-up operation mode at $f_{sw}$ = 85 kHz

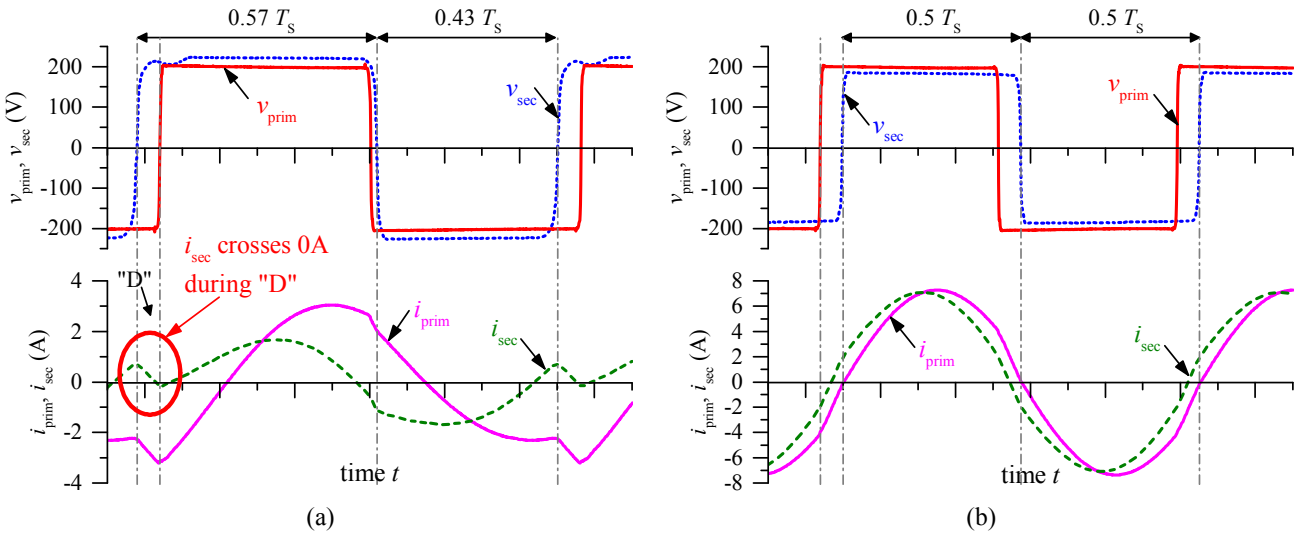


Fig. 6. Measured current and voltage waveforms of the resonant tank for step-up operation mode (a) at $f_{sw}$ = 88 kHz and step-down operation mode (b) at $f_{sw}$ = 105 kHz for Si super-junction MOSFET (IPW65R110CFD) used as secondary bridge rectifier.

for the SiC SBD in Fig. 5(a) starts with the power transferring subinterval P at $t = t_0$ and is followed by subinterval N at $t = t_1$, in which the power transfer to the secondary side diminishes and energy is stored in the resonant tank [17]. The rising edge of $v_{sec}$ is very steep due to the very small diode junction capacitance and thus the state of the output rectifier abruptly changes. However, increasing the diode junction capacitance leads to the new subinterval D, in which the capacitances are charged and discharged by the secondary resonant current $i_{sec}$. For the PN operating mode, subinterval D emerges between subinterval P and N as $i_{sec}$ crosses zero at $t = t_1$ and the secondary rectifier begins to alter polarity. Due to the diode junction capacitances an instantaneous transition is not possible compared to ideal devices. At $t = t_1$ all four rectifier diodes begin to block and $i_{sec}$ starts to charge $C_{j5}$ and $C_{j8}$, resp. discharge $C_{j6}$ and $C_{j7}$ (see Fig. 1). After $C_{j6}$ and $C_{j7}$ are discharged down to the diode forward voltage at $t = t_2$, the diodes $D_6$ and $D_7$ begin to conduct and subinterval D ends. No output current and thus no output power is transferred to the secondary side during this subinterval. Moreover, from Fig. 5(a) it can be clearly seen that the insertion of subinterval D shortens in step-up mode the period length of N. Furthermore, in stage D the voltage across the complete resonant network $v_{tank} = v_{prim} - v_{sec}$ slowly rises with the same gradient the diode junction capacitances are discharged. In comparison to the ideal device, the combination of subinterval D and N results in a smaller voltage-time product $v_{tank} \cdot (t_3 - t_1)$ and thus in less stored energy in the resonant tank. In the following subinterval P less energy can be transferred to the load resulting in a decrease of $i_{prim}$, $i_{sec}$, and the output power $p_{out}$ for increasing values of $C_{add}$.

### C. New subinterval D in step-down operation mode

In contrast, the subinterval order in step-down operation mode is reversed as shown in Fig. 5(b). Here, at $f_{sw}$ = 105 kHz the first half-cycle of the switching period starts with subinterval N at $t = t_0$, followed by subinterval P at $t = t_2$ for the SiC SBD without additional capacitance. Again, for the SiC SBD the secondary resonant voltage $v_{sec}$ rises rapidly from $-V_2$ to $+V_2$. For the SiC SBD with additional capacitance $C_{add}$ the new subinterval D emerges between N and P, starting at $t = t_1$ with the zero-crossing of $i_{sec}$ and ending at $t = t_2$ once the capacitances $C_{j5}$ and $C_{j8}$ are discharged ($C_{j6}$ and $C_{j7}$ are charged, respectively). For this reason, the discharging process in subinterval D extends the length of the preceding subinterval N as can be seen in Fig. 5(b). This results in a larger voltage-time product $v_{tank} \cdot (t_2 - t_0)$ and thus leading to a higher stored energy in the resonant tank and to a higher output power in the subsequent subinterval P. Hence, $p_{out}$ and the peak values of $i_{prim}$ and $i_{sec}$ increase with rising diode junction capacitance values.

### D. Special behavior of Si MOSFET

Next, the remarkable behavior of the Si MOSFET is shortly explained. As already described, the super-junction Si MOSFET features a large transistor output capacitance. In addition, the internal capacitances of Si devices exhibit a strong nonlinear charge-voltage (CV) characteristic depending on device technology [23]. In Fig. 6(a) the measured current and voltage waveforms at the observed discontinuity (see Fig. 2(b)) at $f_{sw}$ = 88 kHz for step-up operation mode is plotted. Due to part load conditions $i_{sec}$ is low at the beginning of subinterval D, decreases further with a negative slope during D and finally crosses zero (red circle in Fig. 6(a)). This results in an interruption of the charging process of $C_{oss}$ and therefore, the secondary rectifier does not switch polarity at the designated instant. Furthermore, the currently negative secondary resonant current $i_{sec}$ starts to discharge the almost charged transistor output capacitances $C_{oss5}$ and $C_{oss8}$ again, which can be seen in the decrease of $v_{sec}$. This process is stopped by the rising edge of $v_{prim}$, which forces $i_{sec}$ to rise. Hence, the following subinterval P is delayed and aborted early by the primary inverter, which switches from $+V_1$ to $-V_1$. The delayed transition of $v_{sec}$ leads to an imbalance of the positive and negative voltage-time product within one period shown in Fig. 6(a). At the examined switching frequency $f_{sw}$ = 88 kHz the period length of $v_{sec} = +V_2$ amounts to 57% of the switching period $T_S$ and the length of $v_{sec} = -V_2$ is 43%, respectively.

Thus, the resonant tank waveforms are not symmetric to a half-cycle of the switching period and the output power characteristic is slightly distorted in comparison to TDS calculation. In contrast, in step-down mode (Fig. 6(b)) a similar behavior was not observed. Here the positive and negative voltage-time product within one period is equal.

## IV. Design Considerations

Based on the results in this paper, power semiconductors with low diode/transistor output capacitance should be applied in the secondary rectifier. This reduces the effect of the diode junction capacitance (the transistor output capacitance, respectively) on output power and hence TDS calculations can be used for converter design. Therefore, recent ultrafast Si and SiC diodes are suitable for rectifier operation with junction capacitance values in the lower picofarad range. Hence, a higher output power is available in step-up mode utilizing a larger area of the limited output power range. In addition, the regulation in the light load range becomes easier in step-down mode due to the lower output level at high switching frequencies. Moreover, the analyzed wide-bandgap bidirectional switches also show low transistor output capacitances. However, in step-up operation mode the resonant tank has to be designed for a higher nominal output power to compensate for the performance drop introduced by the diode junction capacitances. Thus, the aspired switching frequency range will slightly change compared to TDS calculations. In contrast to step-up operation mode, in step-down mode the influence of the diode junction capacitance is less critical because of the very high output power capability around the series resonance. But, as a result the operating frequency range will slightly change to achieve the desired output power. Moreover, for diodes or transistors with high output capacitance values the regulation of light and very light load conditions can be achieved e.g. by applying pulse skipping control method.

## V. Conlusion

This paper demonstrates that the secondary side rectifier diodes junction capacitance has a significant influence on converter output power. The influence is analyzed on the basis of experimental results using a CLLLC topology in an exemplary IPT system. In addition to current Si power semiconductors, wide-bandgap (SiC, GaN) diodes and transistors are analyzed to cover all current state of the art semiconductor devices. The individual operating modes and also voltage and current waveforms of the resonant tank in step-up and step-down operation mode are discussed in detail. Based on these results, practical design considerations for the CLLLC resonant converter are provided.

## Acknowledgment

This contribution was supported by the Bavarian Ministry of Economic Affairs and Media, Energy and Technology as a part of the Bavarian project ”Leistungszentrum Elektroniksysteme (LZE)”. The authors would like to thank Dr. S. Ditze, Cluster of Excellence Engineering of Advanced Materials (EAM) for her valuable scientific input.

## References

[1] S. Johnson and R. Erickson, “Steady-state analysis and design of the parallel resonant converter,” IEEE Transactions on Power Electronics, vol. 3, no. 1, pp. 93-104, 1988.

[2] R. Liu, C. Lee, and A. Upadhyay, “Experimental study of the LLC-type series resonant converter,” in IEEE 1991 Applied Power Electronics Conference and Exposition (APEC), 1991, pp. 31-37.

[3] S. Johnson, A. Witulski, and R. Erickson, “Comparison of resonant topologies in high-voltage DC applications,” IEEE Transactions on Aerospace and Electronic Systems, vol. 24, no. 3, pp. 263-274, 1988.

[4] M. Mao, D. Tchobanov, D. Li, and M. Maerz, “Design of a 1 MHz half-bridge CLL resonant converter”, IET Power Electronics, vol. 1, no.1, pp. 100-108, March 2008.

[5] A. Hillers, D, Christen, and J. Biela, “Design of a highly efficient bidirectional isolated LLC resonant converter,” in IEEE 2012 International Power Electronics and Motion Control Conference (EPE/PEMC), 2012, pp. DS2b.13 1-8.

[6] R. Beiranvand, B. Rashidian, M. R. Zolghadri, S. M. H. Alavi, “Using LLC Resonant Converter for Designing Wide-Range Voltage Source,” IEEE Transactions on Industrial Electronics, vol. 58, no. 5, pp. 1746-1756, May 2011.

[7] Z. Zhang, Z. Tang, “Pulse frequency modulation LLC series resonant X-ray power supply,” in IEEE 2011 International Conference on Consumer Electronics, Communications and Networks (CECNet) ), 2011, pp. 1532-1535.

[8] J. Jung, H. Kim, M. Ryu, J. Baek, “Design Methodology of Bidirectional CLLC Resonant Converter for High Frequency Isolation of DC Distribution Systems,” IEEE Transactions on Power Electronics, vol. 28, no. 4, pp. 1751-1755, 2012

[9] W. Chen, P. Rong, and Z. Lu, “Snubberless bidirectional dc-dc converter with new CLLC resonant tank featuring minimized switching loss,” IEEE Trans. Ind. Electron., vol. 57, no. 9, pp. 3075–3086, 2010.

[10] Z. U. Zahid, Z. Dalala, L. Jih-Sheng, “Design and control of bidirectional resonant converter for Vehicle-to-Grid (V2G) applications,” in IEEE 2014 Annual Conference on IEEE Industrial Electronics Society (IECON), 2014, pp. 1370-1376.

[11] W. Zhang, S.-C. Wong, C. K. Tse, and Q. Chen, “Analysis and comparison of secondary series- and parallel-compensated inductive power transfer systems operating for optimal efficiency and load-independent voltage-transfer ratio,” IEEE Transactions on Power Electronics, vol. 29, no. 6, pp. 2979-2990, Jun. 2014.

[12] A. Ecklebe and A. Lindemann, “Analysis and design of a contactless energy transmission system with flexible inductor positioning for automated guided vehicles,” in IEEE 2006 Annual Conference on IEEE Industrial Electronics Society (IECON), 2006, pp. 1721-1726.

[13] C. Joffe, S. Ditze, and A. Rosskopf, “A novel positioning tolerant inductive power transfer system,” in IEEE 2013 Electric Drives Production Conference (EDPC), 2013, pp. 1-7.

[14] R. M. Miskiewicz, A.J. Moradewicz, and M.P. Kazmierkowski, “Contactless battery charger with bi-directional energy transfer for plug-in vehicles with vehicle-to-grid capability,” in IEEE 2011 International Symposium on Industrial Electronics (ISIE), 2011, pp. 1969–1973.

[15] R. Steigerwald, “A comparison of half-bridge resonant converter topologies,” IEEE Transactions on Power Electronics, vol. 3, no. 2, pp. 174-182, 1988.

[16] J. Lazar and R. Martinelli, “Steady-state analysis of the LLC series resonant converter,” in IEEE 2001 Applied Power Electronics Conference (APEC), 2001, pp. 728-735.

[17] S. Ditze, “Steady-state analysis of the bidirectional CLLLC resonant converter in time domain,” in IEEE 2014 Telecommunications Energy Conference (INTELEC), 2014, pp. 1-9.

[18] H. Chen and X. Wu, “Analysis on the influence of the secondary parasitic capacitance to ZVS transient in LLC resonant converter,” in IEEE 2014 Energy Conversion Congress and Exposition (ECCE), 2014, pp. 4755-4760.

[19] J.-H. Kim, C.-E. Kim, J.-K. Kim, and G.-W. Moon, “Analysis for LLC resonant converter considering parasitic components at very light load,”

in IEEE 2011 International Conference on Power Electronics (ECCE Asia), 2011, pp. 1863-1868.

[20] B.-H. Lee, M.-Y. Kim, C.-E. Kim, K.-B. Park, and G.-W. Moon, "Analysis of LLC resonant converter considering effects of parasitic components," in IEEE 2009 Telecommunications Energy Conference (INTELEC), 2009, pp. 1-6.

[21] C.-H. Yang, T.-J. Liang, K.-H. Chen, J.-S. Li, and J.-S. Lee, "Loss analysis of half-bridge LLC resonant converter," in IEEE 2013 Future Energy Electronics Conference (IFEEC), 2013, pp. 155-160.

[22] K.-B. Park, B.-H. Lee, G.-W. Moon, and M.-J. Youn, "Analysis on center-tap rectifier voltage oscillation of LLC resonant converter," IEEE Transactions on Power Electronics, vol. 27, no. 6, pp. 2684-2689, Jun. 2012.

[23] R. Elferich, "General ZVS half bridge model regarding nonlinear capacitances and application to LLC design," in IEEE 2012 Energy Conversion Congress and Exposition (ECCE), 2012, pp. 4404-4410.

[24] J. Stahl, D. Kuebrich, T. Duerbaum, A. Leicht, J. Patz, "A fully automated measurement set-up for the determination of the reverse recovery behaviour of ultra-fast diodes," in IEEE 2011 European Conference on Power Electronics and Applications (EPE), 2012, pp. 1-9.

[25] J. Lutz, H. Schlangenotto, H. Scheuermann, R. De Doncker, "Schottky Diodes," in *Semiconductor Power Devices*, 2nd ed. Springer-Verlag Berlin Heidelberg, 2011.

[26] H. Mitlehner, W. Bartsch, M. Bruckmann, K. O. Dohnke, U. Weinert, "The potential of fast high voltage SiC diodes," in IEEE 1997 Power Semiconductor Devices and IC´s (ISPSD), 1997, pp. 165-168.

[27] T. Heckel, B. Eckardt, M. März, L. Frey, "SiC MOSFETs in Hard-Switching Bidirectional DC/DC Converters," in Materials Science Forum, Vols. 821-823, pp. 689-692, Jun. 2015.

[28] N. Kaminski, "State of the art and the future of wide band-gap devices," in IEEE 2009 Power Electronics and Applications (EPE), 2009, pp. 1-9.

[29] X. Huang, Z. Liu, Q. Li. F. C. Lee "Evaluation and Application of 600 V GaN HEMT in Cascode Structure," IEEE Transactions on Power Electronics, vol. 29, no. 5, pp. 2453-2461, May 2014.